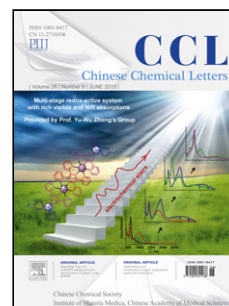# Journal Pre-proof

Needle-like cobalt phosphide arrays grown on carbon fiber cloth as a binder-free electrode with enhanced lithium storage performance

Ze Zhang, Peipei Zhu, Chao Li, Ji Yu, Jianxin Cai, Zhenyu Yang

Please cite this article as: { doi: https://doi.org/

This is a PDF file of an article that has undergone enhancements after acceptance, such as the addition of a cover page and metadata, and formatting for readability, but it is not yet the definitive version of record. This version will undergo additional copyediting, typesetting and review before it is published in its final form, but we are providing this version to give early visibility of the article. Please note that, during the production process, errors may be discovered which could affect the content, and all legal disclaimers that apply to the journal pertain.

Communication

Needle-like cobalt phosphide arrays grown on carbon fiber cloth as a binder-free electrode with enhanced lithium storage performance

Ze Zhang[a], Peipei Zhu[b,*], Chao Li[c], Ji Yu[a], Jianxin Cai[a], Zhenyu Yang[a,*]

[a] *College of Chemistry, Nanchang University, Nanchang 330031, China*
[b] *College of Chemistry and Chemical Engineering, Jiangxi Normal University, Nanchang 330022, China*
[c] *School of Chemical Engineering and Energy Technology, Donogguan University of Technology, Dongguan 523808, China*

∗ Corresponding authors.
 E-mail addresses*: ppzhu@jxnu.edu.cn (P. Zhu), zyyang@ncu.edu.cn (Z. Yang)*

Graphical abstract
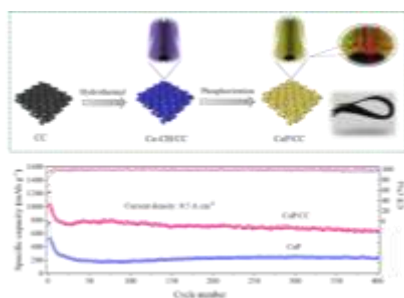
An integrated binder-free electrode featuring with needle-like CoP arrays grown on carbon fiber cloth substrate was reported as an anode material with enhanced lithium storage performance.

ABSTRACT
Cobalt phosphide (CoP) is a promising anode candidate for lithium-ion batteries (LIBs) due to its high specific capacity and low working potential. However, the poor cycling stability and rate performance, caused by low electrical conductivity and huge volume variation, impede the further practical application of CoP anode materials. Herein, we report an integrated binder-free electrode featuring needle-like CoP arrays grown on carbon fiber cloth (CC) for efficient lithium storage. The as-prepared CoP/CC electrode integrates the advantages of 1D needle-like CoP arrays for efficient electrolyte wettability and fast charge transportation, and 3D CC substrate for superior mechanical stability, flexibility and high conductivity. As a result, the CoP/CC electrode delivers an initial specific capacity of 1283 mAh/g and initial Coulombic effeciencies of 85.4%, which are much higher than that of conventional CoP electrode. Notably, the CoP/CC electrode shows outstanding cycling performance up to 400 cycles at 0.5 A/cm^2 and excellent rate performance with a discharge capacity of 549 mAh/g even at 5 A/cm^2. This work demonstrates the great potential of integrated CoP/CC hybrid as efficient bind-free and freestanding electrode for LIBs and future flexible electronic devices

Keywords: Needle-like arrays, CoP, Carbon fiber cloth, Binder-free electrode, Enhanced lithium storage

Rechargeable lithium-ion batteries (LIBs) have attracted much attention due to their advantages of high energy and power density, low energy consumption, and environmental friendliness [1-3]. As a crucial part of LIBs, anode material plays an important role in regulating the battery performance. At present, graphite is the most widely commercial anode due to its high reversibility and low lithiation potential. However, it offers a limited capacity of 372 mAh/g according to the Li$^+$-ion intercalation mechanism [4,5], which makes it cannot meet the great demands of the high-energy devices. Thus, it is an urgent priority to explore the "beyond Li-ion intercalation" mechanism of advanced anode materials to boost specific capacity and energy.

Currently, various types of transition-metal compound based anode materials are investigated for LIBs, including oxides [6-8], sulfides [9,10], and phosphides [11,12]. Among them, transition-metal phosphides (TMPs) have been widely researched as promising anodes due to their high capacity, relatively low working potential [13]. For example, cobalt phosphide (CoP) anode material can afford high theoretical specific capacity of ~826 mAh/g [14], which is more than two times that of graphite anode. Despite the lower capacity compared with anodes such as Si or Sn-based materials, and Li metal, CoP anode, however, shows much lower volume variation than Si or Sn-based anodes, and better safety issue than Li metal anode. On the hand, the poor electronic conductivity and volume variation during charge/discharge processes still restrict the electrochemical performance of CoP anode materials [15]. To solve these issues, rational construction of CoP-based hybrid nanostructures is urgently needed for high-performance LIBs. In particular, a three-dimensional (3D) architectural structure with large surface area and abundant active sites is preferred to promote lithium reaction, enable sufficient electrolyte access, and show promising mechanical stability to buffer the volume expansion for advanced electrodes

[16,17]. More importantly, such 3D structures can be employed as integrated and bind-free electrode of flexible LIBs for next-generation flexible and portable electronic devices [18,19]. Specifically, various substrates including carbon nanotubes and graphene have been researched for constructing flexible electrodes [20,21]. Despite of their excellent electrochemical properties, the poor mechanical stability limits their wide applications in practical devices. In this connection, carbon fiber cloth has been widely used as a flexible substrate with desirable characteristics including low cost, mechanical flexibility, high conductivity and robustness for bind-free electrode for electrochemical energy storage [22,23].

Herein, we report needle-like CoP arrays grown on a carbon fiber cloth (denoted as CoP/CC) as an integrated bind-free anode with enhanced lithium storage performance. In the hybrid, the interconnected conductive network of CC provides fast electron transportation pathways and migrates the volume change to maintain the structural integrity of the electrode due to its mechanical stability and strength. Meanwhile, the one-dimensional (1D) needle-like CoP arrays enable sufficient contact with electrolyte and numerous active sites, and also effectively reduce the transport path of lithium ions. As a result, the flexible binder-free CoP/CC electrode shows high specific capacity, improved cycle stability, and high rate performance.

As illustrated in Fig. 1a, the integrated binder-free CoP/CC electrode was obtained *via* a hydrothermal method following with the phosphorization process. The detailed preparation can be seen in the Supporting Information. Specifically, needle-like Co-precursor arrays grow on the flexible CC substrate after a hydrothermal route. After a subsequent phosphorization process, the Co-precursor transforms to CoP, and maintains the needle-like structure. Notably, the as-obtained CoP/CC electrode exhibits good flexibility. Figs. 1b and c show the scanning electron microscopy (SEM) images with different magnifications of Co-precursor/CC, demonstrating that the precursor exhibits a needle-like array structure. The precursor arrays fully and uniformly root on the CC surface and grow along the radial direction of carbon fibers. After phosphating, the needle-like morphology is well retained only with a little twist (Figs. 1d and e) for the CoP/CC sample. The needle-like structure can also be obtained without the addition of CC substrate, as seen in the SEM image of powder Co-precursor sample (Fig. S1a in Supporting information). However, it suffers severe pulverization and agglomeration after the phosphorization (Fig. S1b in Supporting information). The results demonstrate the positive role of CC substrate in maintaining the morphology of CoP arrays during the phosphorization. In addition, energy-dispersive X-ray spectroscopy (EDXS) mapping in Fig. 1f reveals that Co and P elements are homogenously distributed along with the carbon fibers. Figs. 1g and h show transmission electron microscope (TEM) images of needle-like CoP, and the clear lattice fringes with an interplane spacing of 0.37 nm are related to the (101) plane of CoP [15], which can also be indexed from the inset fast Fourier transformation (FFT) based on orthorhombic CoP.
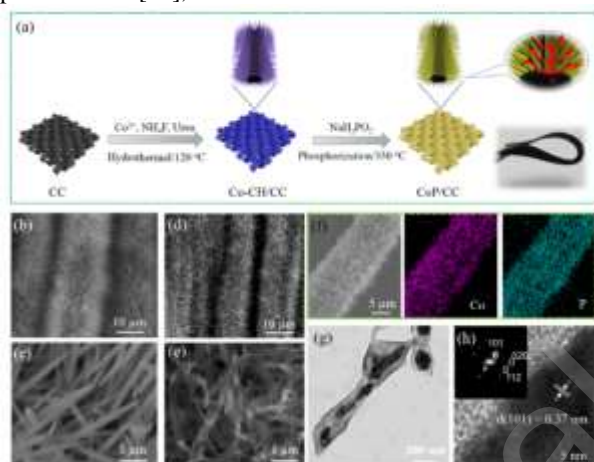

Fig. 1. (a) Schematic illustration of preparation of CoP/CC. SEM images of (b,c) Co-precursor/CC and (d,e) CoP/CC. (f) SEM image of CoP/CC and EDXS elemental mapping of Co and P. (g) TEM and (h) high-resolution TEM image of CoP/CC. Inset shows the fast Fourier transformation (FFT) pattern.

The phase purities of Co-precursor/CC and CoP/CC samples are determined by X-ray diffraction (XRD) in Figs. 2a and b. All peaks of Co-precursor (Fig. 2a) are assigned to the orthorhombic $Co(CO_3)_{0.5}(OH)\cdot0.11H_2O$ (JCPDS No. 48-83), except the broad peaks of CC substrate. In the case of CoP/CC, all the diffraction peaks can be indexed as an orthorhombic CoP structure (JCPDS No. 65-2593) with no significant impurity peaks, as well as the control CoP powder sample (Fig. S2 in Supporting information). The results suggest the successful preparation of pure CoP. Furthermore, Raman spectrum of CoP/CC (Fig. 2c) shows typical bands located at around 1341 and 1586 cm^{-1}, which are attributed to the pyrrole ring and C=C backbone stretching, respectively [24,25]. The peak at 677 cm^{-1} belongs to the chemical bonding between Co and P in CoP [26]. The results indicate the coexistence of CoP and carbon component in CoP/CC. Thermogravimetric analysis (TG) curve of CoP/CC under air atmosphere is shown in Fig. 2d. According to the content of about 33.2 wt% for the residue $Co_2P_2O_7$ [15], the content of CoP in CoP/CC can be calculated as 20.5 wt% in CoP/CC.

The surface chemical compositions of CoP/CC sample are identified by X-ray photoelectron spectroscopy (XPS). The Co 2p spectrum in Fig. 2e presents two spin-orbit doublets of Co $2p_{3/2}$ and Co $2p_{1/2}$ with two corresponding representative satellite peaks. The doublet peaks at binding energies of 779.6 eV and 797.7 eV are attributed to Co-P bond in CoP, while the peaks at 782.4 eV and 799.0 eV are related to Co-O bond due to the surface oxidation of CoP [27]. The P 2p spectrum in Fig. 2f exhibits two peaks at 129.9 and 130.6 eV, which were ascribed to P $2p_{1/2}$ and P $2p_{3/2}$ in CoP [28], respectively. Moreover, the broad peak observed at 134.0 eV is attributed to the oxidized P caused by the surface oxidation.
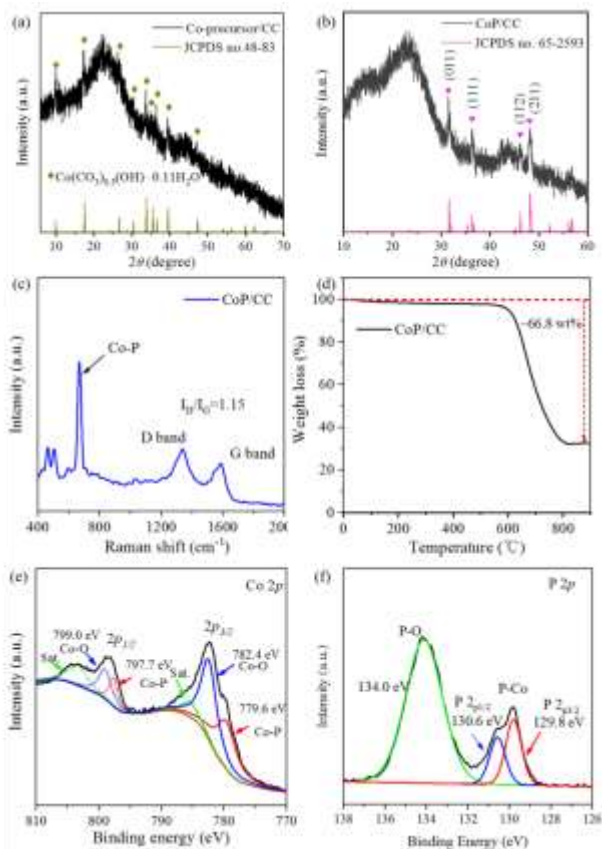
Fig. 2. XRD patterns of (a) Co-precursor/CC and (b) CoP/CC. (c) Raman spectrum, (d) TG curve, (e) Co 2p and (f) P 2p XPS spectra of CoP/CC.

Fig. 3a shows the galvanostatic charge/discharge profiles of the binder-free CoP/CC electrode at 0.1 A/cm² from 0.02 V to 3.0 V. The first discharge curve shows three platforms around 1.2 V, 0.6 V and 0.01 V. The first plateau at 1.2 V is associated with the formation of solid electrolyte interface (SEI) layer originated from the electrolyte decomposition. The subsequence plateau at 0.6 V is related to the insertion of Li⁺ ions into CoP, leading to the formation of a transition phase Li_xCoP [29]. The third plateau around 0.01 V is attributed to the further reduction of Li_xCoP to Co and Li_3P [30]. The conversion from CoP to Co substances induces high specific capacity. It can be observed that the initial discharge and charge capacities reach about 1283 mAh/g and 1096 mAh/g, leading to a high initial Coulombic efficiency of 85.4%. The above conversion reaction process can be expressed as following:

$$CoP + xLi^+ + e^- \rightarrow Li_xCoP \tag{1}$$
$$Li_xCoP + (3-x)Li^+ + e^- \rightarrow Li_3P + Co \tag{2}$$
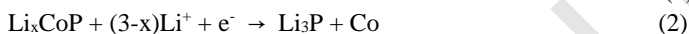
In the case of conventional CoP electrode (Fig. S3 in Supporting information), the initial discharge capacity and Coulombic efficiency are much lower than the binder-free CoP/CC electrode, demonstrating the positive role in enhancing the active utilization of CC substrate due to its highly conductive structure. The conductive CC substrate benefits for rapid charge transfer within CoP/CC electrode due to lower resistances, as shown in the electrochemical impedance spectroscopy (EIS) profiles (Fig. S4 in Supporting information). In the subsequent cycles, CoP/CC electrode exhibits higher reversible specific capacity of 1016 mAh/g and 1000 mAh/g (in 2ⁿᵈ and 3ʳᵈ cycle) than that of the conventional CoP electrode (669 mAh/g and 623 mAh/g), indicating efficient active material utilization of the binder-free CoP/CC electrode. Cyclic voltammogram (CV) curves are further measured to probe the electrochemical process. As shown in Fig. 3b, the CoP/CC electrode exhibits two anodic peaks located at around 1.2 V in the first charge scan, assigned to the transformation of Li_3P to CoP. While the high peak located at 0.3 V should be related to the deintercalation of Li⁺ ions from the CC substrate according to the CV curves of pristine CC (Fig. S5 in Supporting information). After the first discharge/charge reaction, the overlapped curves adumbrate the good electrochemical reversibility and stability of CoP/CC electrode. In the subsequent cycles, the main reduction peaks were shifted to 0.67 V, which might result from the activation and redistribution of CoP materials during the initial cathodic scan. Notably, the CV curves of conventional CoP electrode (Fig. S6 in Supporting information) are similar to that of CoP/CC except that the redox peaks of pristine CC substrate are not observed, and the redox peaks positions of the 2ⁿᵈ and 3ʳᵈ cycle shift slightly [31]. More importantly, CV curves of CoP/CC electrode are more stable after the initial cycle than conventional electrode, indicating that the conductive CC substrate induces better electrochemical reaction kinetics.

Fig. 3c shows the cycle stability of the two electrodes at a current density of 0.1 A/cm² over 200 cycles. CoP/CC electrode shows a high capacity retention of 82.0% with the capacities decreasing from 1097 mAh/g at the 2ⁿᵈ cycle to 900 mAh/g at 200ᵗʰ cycle, while the capacity retention of conventional CoP electrode is much lower as ~51.8% with the capacities decreasing from 657 mAh/g (2ⁿᵈ cycle) to 340 mAh/g after 200 cycles. In addition, the binder-free CoP/CC electrode exhibits higher average Coulombic efficiency of ~99.8% than that of conventional CoP electrode (~98.2%) over 200 cycles. The rate capability in Fig. 3d demonstrates that CoP/CC electrode shows excellent rate capability with a high discharge capacity of 549 mAh/g even at 5 A/cm², which is much higher than that of 75 mAh/g for conventional CoP electrode. When the current density reaches back to 0.1 A/cm², the specific discharge capacity of CoP/CC electrode recovers to 940 mAh/g. Significantly, the CoP/CC electrode demonstrates excellent cycle durability and high initial coulombic efficiency of 84.1% (Fig. 3e) at 0.5 A/cm². Notably, the phenomenon that the capacity increases in the initial cycles is a result of an activation process [32]. The discharge capacity maintains as 629 mAh/g after 400 cycles with the low decay rate of ~0.98% per cycle. In contrast, the conventional CoP electrode exhibits lower reversible capacity of 526 mAh/g and the capacity rapidly

decreases to 235 mAh/g. Given that the reversible capacity contribution of pristine CC substrate (only 150 mAh/g at 0.1 A/cm^2, and 100 mAh/g at 0.5 A/cm^2), as seen in Fig. S7 (Supporting information), the capacity of binder-free CoP/CC electrode still exceeds to that of conventional CoP electrode. The results clearly demonstrate the excellent rate capability and remarkable cycle stability of the binder-free CoP/CC electrode. It should be noted that the high capacity retention (82.0% after 200 cycles) and high initial Coulombic efficiency (84.1%) are achieved for the binder-free needle-like CoP arrays/CC electrode with an extremely high specific loading (3.5 mg/cm^2) of active CoP material, which outperforms most reported CoP-based anode materials [14,15,29,30,33-43], as concluded in Table S1 (Supporting information).
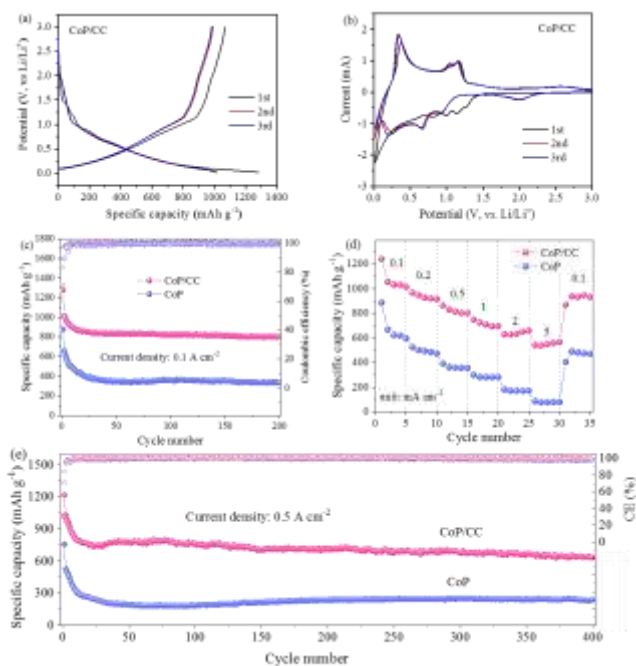

Fig. 3. (a) Galvanostatic charge/discharge profiles and (b) CV curves of CoP/CC electrode. (c) Cycle performance at 0.1 A/cm^2, (b) rate capability, and (c) long-term cycling performance at 0.5 A/cm^2 of conventional CoP electrode and binder-free CoP/CC electrode.

The enhanced lithium storage performance of CoP/CC electrode is related to the 3D conductive and stable structure of CC substrate. As shown in Fig. 4, the SEM images (Figs. 4a and b) of the cycled CoP/CC electrode demonstrate that needle-like CoP arrays still maintain well on the CC surface without obvious peeling off, indicating the outstanding structure integrity during cycling. Furthermore, the EDXS mappings in Figs. 4c and d demonstrate that the elements of Co and P homogenously distribute along with the carbon fibers. Even after cycling at a higher current density (0.5 A/cm^2) for 400 cycles, the active CoP materials still adhere tightly onto the carbon fibers with a homogenous element distribution (Fig. S8 in Supporting information), indicating the excellent structural stability. Thus, the superior electrochemical performance of binder-free CoP/CC electrode can be ascribed to the particular structure of 1D needle-like arrays on flexible CC substrate, which can suppress the aggregation of CoP nanoneedles over the continuous cycling, improve the electrical conductivity, and retain the structure integrity of the CoP/CC electrode. Therefore, the flexible binder-free CoP/CC electrode can realize high active material utilization and high-rate performance.
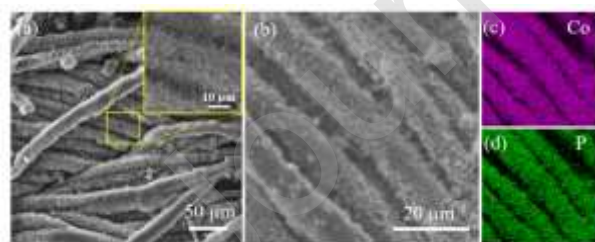

Fig. 4. (a,b) SEM image and (c,d) EDXS mapping of the CoP/CC electrode after 200 cycles at 0.1 A/cm^2.

In summary, a novel integrated binder-free CoP/CC electrode featuring with needle-like CoP arrays grown on CC substrate is reported for LIBs. Compared with conventional CoP electrode, the binder-free CoP/CC electrode demonstrates high reversible capacity, excellent rate performance, and outstanding cycling performance with a reversible capacity of 629 mAh/g after 400 cycles. The excellent electrochemical properties are ascribed to the following advantages of CoP/CC electrode. Firstly, 3D conductive CC substrate provides fast electron transport pathways, and exhibits excellent mechanical stability to maintain the structure integrity of electrode during cycling. Secondly, needle-like CoP arrays grown on carbon fibers enable sufficient electrolyte access and numerous active sites. Thirdly, the flexible CoP/CC electrode avoids the utilization of nonconductive and inactive binder to increase the conductivity of electrode. Therefore, the flexible bind-free CoP/CC hybrid offers great potential as anode material with superior performance for LIBs and future flexible electronic devices.

Declaration of competing interest

Acknowledgments

References

[1] N.S. Choi, Z.H. Chen, S.A. Freunberger, et al., Angew. Chem. Int. Ed. 51 (2012) 9994-10024.
[2] D. Larcher, J.M. Tarascon, Nature Chem.7 (2015) 19-29.
[3] Z. Zhang, D.H. Wu, Z. Zhou, G.R. Li, S. Liu, X.P. Gao, Sci. China Mater. 62 (2019) 74-86.
[4] K. Feng, M. Li, W.W. Liu, et al., Small 14 (2018) 1702737.
[5] J.D Luo, H. Zhang, Z. Zhang, J. Yu, Z.Y. Yang, Carbon 155 (2019) 1-8.
[6] J.D. Luo, H. Zhang, X.T. Qi, et al., Carbon 162 (2020) 36-45.
[7] H. Zhang, Z. Zhang, J.D. Luo, et al., ChemSusChem 12 (2019) 283-290.
[8] G.Y. Zeng, H. Wang, J. Guo, et al., Chin. Chem. Lett. 28 (2017) 755-758.
[9] L. Wu, J. Zheng, L. Wang, et al., Angew. Chem. Int. Ed. 58 (2019) 811-815.
[10] Z.Y. Guo, Y. Zhong, Y. Liu, C.M. Mao, G.C. Li, Chin. Chem. Lett. 28 (2017) 743-747.
[11] P.P. Zhu, Z. Zhang, S.J. Hao, et al., Carbon 139 (2018) 477-485.
[12] C. Wu, P. Kopold, P.A. Van Aken, et al., Adv. Mater. 29 (2017) 1604015.
[13] G.A. Li, C.Y. Wang, W.C. Chang, H.Y. Tuan, ACS Nano 10 (2016) 8632-8644.
[14] L.S. Ni, G. Chen, X.H. Liu, et al., ACS Appl. Energy Mater. 11 (2019) 406-412.
[15] P.P. Zhu, Z. Zhang, P.F. Zhao, et al., Carbon 142 (2019) 269-277.
[16] F. Han, C.Z. Zhang, J.X. Yang, et al., J. Mater. Chem. A 4 (2016) 12781-12789.
[17] P.L. He, X.Y. Yu, X.W. Lou, Angew. Chem. Int. Ed. 129 (2017) 3955-3958.
[18] N. Li, Z.P. Chen, W.C. Ren, F. Li, H.M. Cheng, Proc. Natl. Acad. Sci. 109 (2012) 17360-17365.
[19] M.S. Balogun, H. Yang, Y. Luo, et al., Energy Environ. Sci. 11 (2018) 1859-1869.
[20] L. Chen, G.M. Zhou, Z.B. Liu, et al., Adv. Mater. 28 (2016) 510-517.
[21] Z.P. Wu, W.T. Qiu, Y.X. Chen, et al., J. Mater. Chem. A 5 (2017) 756-764.
[22] S.H. Shen, S.J. Deng, Y. Zhong, et al., Chin. Chem. Lett. 28 (2017) 2219-2222.
[23] S.X. Fu, L.P. Li, L.S. Meng, et al., Mater. Chem. Front. 4 (2020) 231-242.
[24] Z. Zhang, A.H. Shao, D.G. Xiong, et al., ACS Appl. Mater. Interfaces 12 (2020) 19572-19580.
[25] D.G. Xiong, Z. Zhang, X.Y. Huang, et al., J. Energy Chem. 51 (2020) 90-100.
[26] C. Tang, R. Zhang, W.B. Lu, et al., Adv. Mater. 29 (2017) 1602441.
[27] Z. Zhang, L.L. Kong, S. Liu, G.R. Li, X.P. Gao, Adv. Energy Mater. 7 (2017) 1602543.
[28] X.W. Lv, W.W. Tian, Y.P. Liu, Z.Y. Yuan, Mater. Chem. Front. 3 (2019) 2428-2436.
[29] Y. Yang, Y.F. Jiang, W.B. Fu, et al., Dalton Trans. 48 (2019) 7778-7785.
[30] J. Yang, Y. Zhang, C.C. Sun, Nano Res. 9 (2016) 612-621.
[31] Y.L. Xu, B. Peng, F. M. Mulder, Adv. Energy Mater. 8 (2018) 1701847.
[32] D. Sun, X.B. Zhu, B. Luo, et al., Adv. Energy Mater. 8 (2018) 1801197.
[33] M.N. Chen, P.Y. Zeng, Y.Y. Zhao, et al., Front. Mater. Sci. 12 (2018) 214-224.
[34] M.M. Du, B.C. Qiu, Q.H. Zhu, et al., Res. Chem. Intermediat. 44 (2018) 7847-7859.
[35] G.H. Jiao, Y. Gu, J. Wang, D. et al., J. Mater. Sci. 54 (2019) 3273-3283.
[36] X.J. Zhao, D. Luo, Y. Wang, et al., Nano Res. 12 (2019) 2872-2880.
[37] Z. Han, B.B. Wang, X.J. Liu, et al., J. Mater. Sci. 53 (2018) 8445-8459.
[38] X.J. Xu, J. Liu, R.Z. Hu, et al., Chem. Eur. J. 23 (2017) 5198-5204.
[39] J. Bai, B.J. Xi, H.Z. Mao, et al., Adv. Mater. 30 (2018) 1802310.
[40] B.B. Wang, K. Chen, G. Wang, et al., Nanoscale 11 (2019) 968-985.
[41] X.X. Wang, Z.L. Na, D.M. Yin, et al., ACS Nano 12 (2018) 12238-12246.
[42] H. Gao, F.H. Yang, Y. Zheng, et al., ACS Appl. Mater. Interfaces 11 (2019) 5373-5379.
[43] S. Sun, T.H. Xie, S. Tao, Energy Technol. 8 (2020) 1901089.